Journal of Alloys and Compounds 509 (2011) 10234–10240

Contents lists available at SciVerse ScienceDirect

Journal of Alloys and Compounds

journal homepage: www.elsevier.com/locate/jallcom

Synthesis of layered birnessite-type manganese oxide thin films on plastic substrates by chemical bath deposition for flexible transparent supercapacitors

Yu Hu, Hongwei Zhu, Jun Wang, Zhenxing Chen*

School of Chemistry and Chemical Engineering, Sun Yat-sen University, Guangzhou 510275, PR China

ARTICLE INFO

Article history:
Received 7 June 2011
Received in revised form 24 August 2011
Accepted 25 August 2011
Available online 3 September 2011

Keywords:
Energy storage materials
Oxide materials
Thin films
Chemical synthesis
Optical properties
Supercapacitor

ABSTRACT

Layered birnessite-type manganese oxide thin films are successfully fabricated on indium tin oxide coated polyethylene terephthalate substrates for flexible transparent supercapacitors by a facile, effective and inexpensive chemical bath deposition technology from an alkaline $KMnO_4$ aqueous solution at room temperature. The effects of deposition conditions, including $KMnO_4$ concentration, initial molar ratio of $NH_3{\cdot}H_2O$ and $KMnO_4$, bath temperature, and reaction time, on the electrochemical properties of MnO_2 thin films are investigated. Layered birnessite-type MnO_2 thin films deposited under optimum conditions display three-dimensional porous morphology, high hydrophilicity, and a transmittance of 77.4% at 550 nm. A special capacitance of 229.2 $F\,g^{-1}$ and a capacitance retention ratio of 83% are obtained from the films after 1000 cycles at 10 $mV\,s^{-1}$ in 1 M Na_2SO_4. Compressive and tensile bending tests show that as-prepared MnO_2 thin film electrodes possess excellent mechanical flexibility and electrochemical stability.

1. Introduction

Supercapacitors have attracted increased attention in recent years due to their high capacitance, long cycle life, and fast charge/discharge rate [1–4]. These performances are especially advantageous for electronic devices, such as MP3 players, laptops, electric toys and solar lighting fixtures. However, nowadays, rigid and opaque coin-type electrodes which are fabricated by the physical mixing of active materials, conductive carbon additives, and polymer binders limit further applications of supercapacitors [5–8]. Thus, for the sake of meeting the rapidly growing modern market requirements, conventional electrochemical capacitors are demanded to develop in the direction of being thin, small, portable and bendable [9–12]. On the one hand, active thin films on flexible substrates are able to reduce devices thickness, leading to lightweight, flexing, and even non-planar shaping. On the other hand, thin film electrodes could be in possession of better electrochemical properties without organic adhesives. Furthermore, as current collects, plastic substrates not only can provide much less mass than metal strips (mainly copper, nickel and stainless steel foils) in roll-to-roll manufacturing processes, but also have excellent optical properties [13–15]. Assembled with field effect transistors, solar cells, Li batteries or fuel cells, respectively, transparent flexible thin film supercapacitors may lead to numerous potential applications in entirely transparent flexible energy conversion and energy storage devices. Therefore, fabricating multifunctional electrochemical capacitors with superiorities of thin, flexible, optically transparent, lightweight and low cost remains a worthwhile endeavor.

Manganese oxide is a promising pseudocapacitive electrode material for electrochemical capacitors because of its low cost, eco-friendly properties, and high theoretical specific capacitance [16–19]. Among all the crystallographic forms of manganese oxide [20–24], the use of birnessite-type MnO_2 has become popular due to its layered structure, which is beneficial for the intercalation and deintercalation of H^+ or alkali metal cations, and shows promising properties in enhancing the special capacitance [25]. Although layered birnessite-type MnO_2 thin films can be prepared by the sol–gel method [26,27], electrostatic spray [28], hydrothermal synthesis [29,30], and electrodeposition [31], large-scale industrial production via these approaches will be limited due to their harsh reaction conditions, energy consuming and complicated procedures. The present work proposes the synthesis of layered birnessite-type MnO_2 thin films directly grown on indium-tin-oxide (ITO)-coated polyethylene terephthalate (PET) substrates at room temperature by a facile, effective and inexpensive chemical bath deposition technique (CBD) for flexible transparent supercapacitor applications. However, few literatures have reported about flexible electrochemical capacitors under bending conditions. And only provided some optical images of the bent electrodes also cannot sufficiently demonstrate the potential applications in bendable supercapacitors [32–35]. Thus, in order to clarify the mechanical flexibility and

* Corresponding author. Tel.: +86 020 84113159.
E-mail address: chenzx65@mail.sysu.edu.cn (Z. Chen).

0925-8388/$ – see front matter © 2011 Elsevier B.V. All rights reserved.
doi:10.1016/j.jallcom.2011.08.080

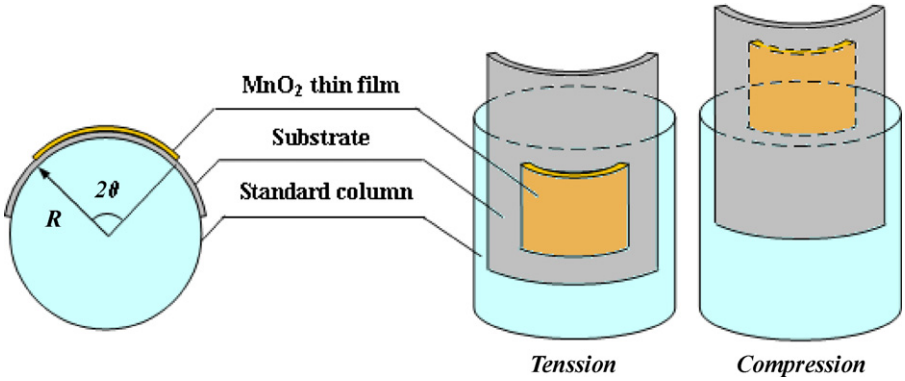

Fig. 1. Schematic details of the flexible transparent electrode in the electrochemical experiments carried out under compressive and tensile bending.

electrochemical stability of as-prepared MnO_2 thin film electrodes, we have systemically studied the efforts of bending angle and flexure count on electrochemical performances, under compressive and tensile strain, respectively, in this paper.

2. Experimental

2.1. Materials

Analytical grade potassium permanganate ($KMnO_4$, >99.5%), aqueous ammonia solution ($NH_3{\cdot}H_2O$, 25 wt%), acetone (>99.7%), and ethanol (>99.7%) were used without further purification. Flexible ITO/PET substrates (90 Ω sq^{-1}) were cleaned in ultrasonic washer with acetone, ethanol, and deionized water for 10 min, respectively, and then dried with purified nitrogen gas.

2.2. Preparation of MnO_2 thin films

MnO_2 thin films were prepared by the CBD method. Clean ITO/PET substrates masked with polyimide tape were vertically immersed in the aqueous solution containing $KMnO_4$ and $NH_3{\cdot}H_2O$. The heterogeneous reaction that occurred on the ITO surface can be represented as follows:

$$2KMnO_4 + 2NH_3{\cdot}H_2O \rightarrow 2MnO_2 + N_2 + 2KOH + 4H_2O$$

After the reaction, the as-prepared MnO_2 thin film electrodes were washed with deionized water and then dried in air for 12 h.

2.3. Physical characterization of MnO_2 thin films

The weight of MnO_2 thin films was measured by a microbalance (Mettler-Toledo, MT5, Greifensee, Switzerland) with an accuracy of 0.01 mg. The surface morphology was examined by a thermal field emission environment scanning electron microscope (TFE-SEM, Quanta 400F, FEI, Netherlands). The crystallinity was analyzed through an X-ray diffractometer (XRD, D-MAX 2200 VPC, Rigaku, Japan) using Cu Kα radiation (λ = 1.5405 nm) with working current and voltage of 30 mA and 40 kV, respectively. Elemental analysis was carried out by inductively coupled plasma emission spectroscopy (ICP-ES, IRIS Intrepid II, Thermo Electron, USA). Thermogravimetric/differential thermal analysis (TG/DTA) was performed on an NETZSCH TG 209F1 Iris machine with a temperature increment of 10 °C min^{-1} in an N_2 environment. The Fourier transform infrared (FT-IR) spectrum was obtained with a Bruker EQUINOX 55 Fourier transform mid-IR spectrometer using the KBr pellet technique. The wettability was determined with a contact angle system (OCA-20, DataPhysics Instruments GmbH, Filderstadt, Germany) at 25 °C. The UV–visible transmittance spectrum was measured with a Shimadzu UV-3150 spectrophotometer.

2.4. Electrochemical characterization of MnO_2 thin film electrodes

The electrochemical characteristics of MnO_2 thin film electrodes were measured in the range of 0–0.7 V by a CHI660B electrochemical workshop (CH instrument, Austin, TX, USA) with a standard three-electrode cell in 1 M Na_2SO_4 at 25 °C. A saturated calomel electrode (SCE) and platinum foil (2.0 cm^2) were used as the reference electrode and counter electrode, respectively. All working electrodes (3.0 cm × 3.0 cm) used in the present study had a geometric area of 1.0 cm × 1.0 cm. The cyclic voltammetry experiments were carried out at scanning rates varied from 1 to 20 mV s^{-1}. The galvanostatic charge/discharge curves were measured at different currents. The mechanical flexibility and electrochemical stability of MnO_2 thin film electrodes were investigated through compressive and tensile bending tests at different bending angles and flexure counts. The flexible transparent working electrode was bent around a series of standard columns and immerged into the electrolyte to test the effects of compressive and tensile strain on electrochemical properties. Bending angles were calculated by radius of columns and the length of the working electrode (1.0 cm). Schematic details of the flexible transparent electrode in the compressive and tensile bending test are shown in Fig. 1.

The specific capacitance and interfacial capacitance of MnO_2 thin films can be calculated by Eqs. (1) and (2), respectively.

$$C_{sp} = \frac{Q}{m \times \Delta V} \quad (1)$$

$$C_{in} = \frac{Q}{S \times \Delta V} \quad (2)$$

where C_{sp} is the specific capacitance (F g^{-1}), Q is the charge, ΔV is the potential window (V), m is the mass of MnO_2 thin film (g), C_{in} is the interfacial capacitance (F cm^{-2}), and S is the apparent area of the working electrode (cm^2).

The specific capacitance of MnO_2 thin films can also be calculated according to Eq. (3).

$$C_{sp} = \frac{I \times \Delta t}{m \times \Delta V} \quad (3)$$

where I is the special current (A) and Δt is the discharge time that can be derived from the plot of galvanostatic charge/discharge cycling at a special current (s).

3. Results and discussion

3.1. Effects of deposition conditions

The effects of deposition conditions, including $KMnO_4$ concentration, initial molar ratio of $NH_3{\cdot}H_2O$ and $KMnO_4$, bath temperature, and reaction time, on the specific capacitance and mass of MnO_2 thin films were investigated through cyclic voltammetry measurements at 10 mV s^{-1} (Fig. 2). The mass of MnO_2 thin films increased and the specific capacitance improved when the $KMnO_4$ concentration, initial molar ratio of $NH_3{\cdot}H_2O$ and $KMnO_4$, bath temperature, and reaction time were all increased. As the reactions progressed, the mass of the films continued to increase. In contrast, the specific capacitance decreased. This variation was attributed to the low electronic and ionic conductivity of MnO_2 films. In other words, electrochemical processes in MnO_2 films are limited by their low electronic conductivity rather than electrolyte accessibility [36,37]. Therefore, to obtain a high specific capacitance, the mass of MnO_2 films must be carefully controlled.

Based on the previous results, the optimum deposition conditions include a $KMnO_4$ concentration of 0.1 M, an initial molar ratio of $NH_3{\cdot}H_2O$ and $KMnO_4$ of 2:1, a bath temperature of 25 °C, and a reaction time of 12 h. Under these conditions, the mass of the prepared MnO_2 thin film obtained was 40 μg cm^{-2}, and the specific capacitance reached 229.2 F g^{-1} at 10 mV s^{-1}.

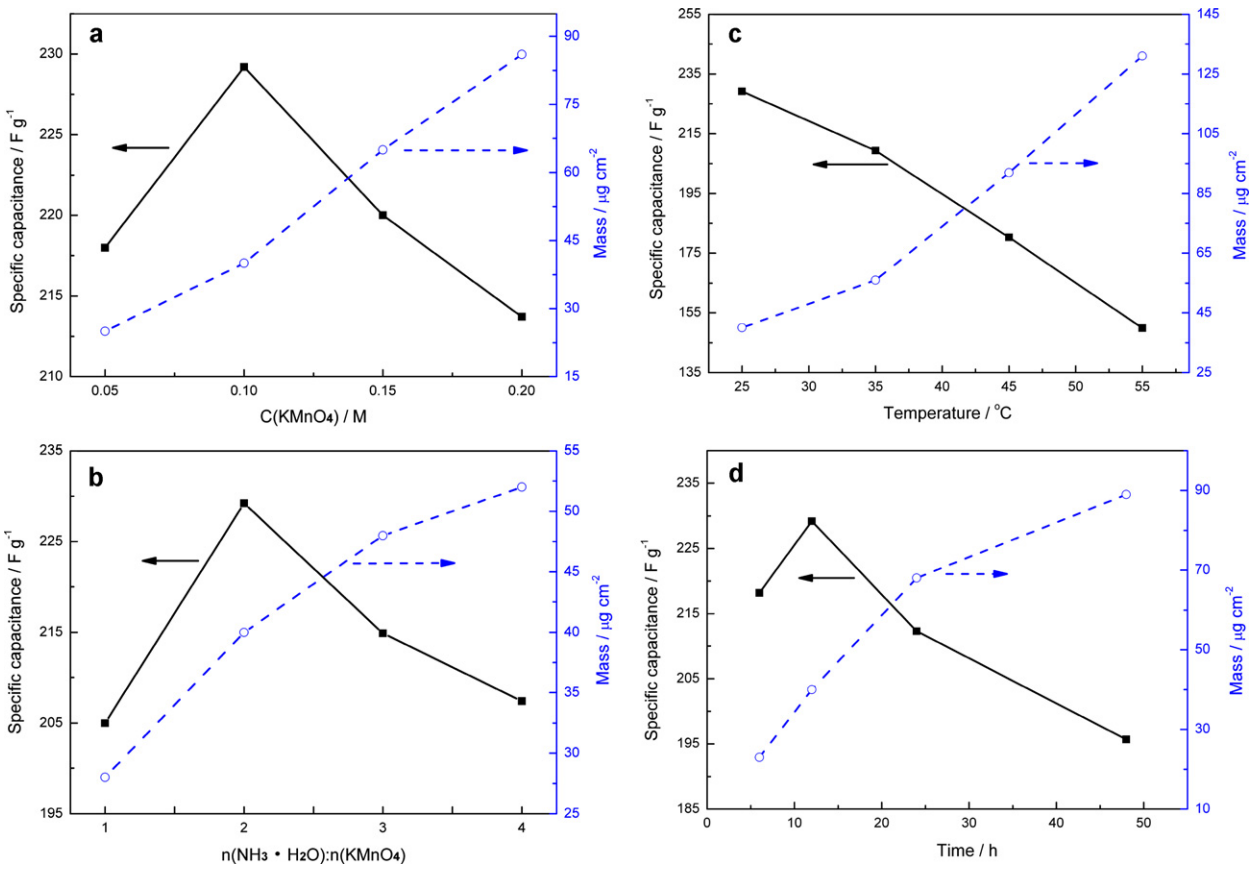

Fig. 2. The specific capacitance (square) and mass (circle) of MnO_2 thin films deposited under the conditions of (a) $n(NH_3{\cdot}H_2O):n(KMnO_4)=2:1$, 25 °C, 12 h; (b) $C(KMnO_4)=0.1$ M, 25 °C, 12 h; (c) $C(KMnO_4)=0.1$ M, $n(NH_3{\cdot}H_2O):n(KMnO_4)=2:1$, 12 h; and (d) $C(KMnO_4)=0.1$ M, $n(NH_3{\cdot}H_2O):n(KMnO_4)=2:1$, 25 °C.

3.2. Characterization of MnO_2 thin films prepared under the optimum conditions

3.2.1. Physical performances

The surface morphology of the MnO_2 thin film presented in Fig. 3 shows the three-dimensional (3D) growth of the spherical beads. The spherical beads were interconnected with each other or aggregated, and the approximate size of the single bead was about 100 nm. Such porous network morphology provides a large surface area, improves ionic conductivity, and facilitates contact between the thin film and the electrolyte. This contact reduces the electrode resistance and accelerates the faradic surface reaction [16,38].

Fig. 4 shows the X-ray diffraction (XRD) patterns of the MnO_2 thin film on and off the ITO/PET substrate. As shown in Fig. 3a, only three intensive peaks related to ITO were observed. This can be ascribed to poor crystallization and the thinness of the MnO_2 film [39]. For MnO_2 powders scraped off from the substrate, four diffraction peaks at 12.3°, 24.9°, 36.6°, and 66.9° (Fig. 4b) were indexed to the pure phase of the layered K-birnessite MnO_2 (JCPDS 52-0556)

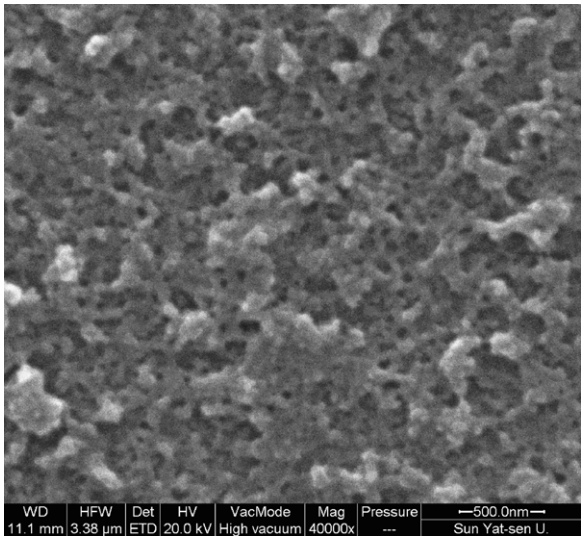

Fig. 3. SEM image of the MnO_2 thin film deposited on the ITO/PET substrate.

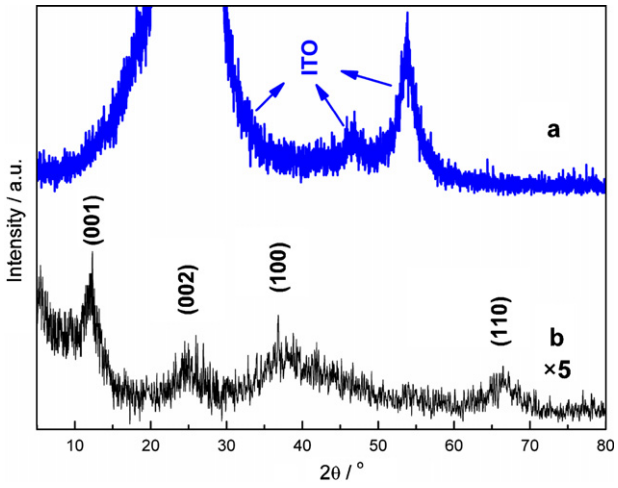

Fig. 4. XRD patterns of the MnO_2 thin film (a) on and (b) off the ITO/PET substrate.

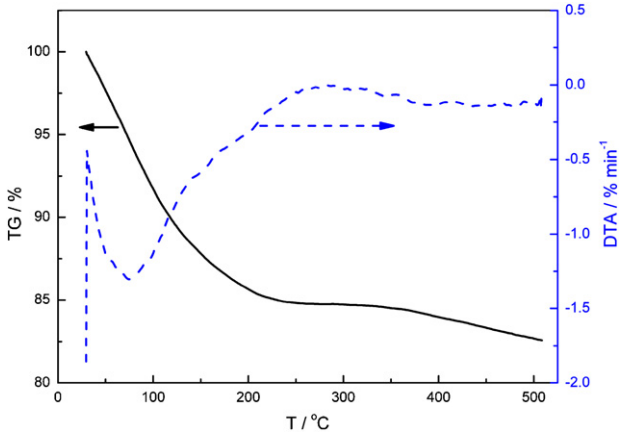

Fig. 5. TG/DTA curves of the MnO_2 powders.

[25,26]. These results indicate that the as-deposited MnO_2 film has a layered structure containing K^+ and H_2O in the interlayer space.

The mass contents of K and Mn were measured by ICP, and the values obtained were 9.07% and 48.86%, respectively. The layered K-birnessite structure of MnO_2 thin films can also be demonstrated by the atom ratio of K/Mn (0.26:1) and the mass content of K [25]. The TG/DTA plots displayed a weight loss of 14.4% between 30 and 200 °C (Fig. 5), corresponding to the loss of physically adsorbed and intercalated water. This finding agrees well with the reported values [29].

Fig. 6 shows the FT-IR absorption spectrum of the MnO_2 powders. A broad –OH stretching vibration peak at 3365 cm^{-1} was indicative of hydrogen-bonded water and the stretching band at 1638 cm^{-1} corresponded to the angular deformation of molecular water [40]. The peaks in the 1000–1600 cm^{-1} region represented vibrations due to the interaction of Mn with its surrounding species, such as –OH, O, H^+, and K^+. Moreover, the absorption peaks at 670 and 525 cm^{-1} revealed the presence of MnO_6 octahedral [41–43].

The wettability of the MnO_2 thin film was determined through water contact angle measurements. The result is shown in Fig. 7. A water contact angle of 34° confirms the hydrophilic behavior of the MnO_2 thin film, which is attributed to the hydroxyl group interaction of Mn atoms with constitutional water within the film structure. The excellent hydrophilicity of the film causes the cations, such as H^+ and Na^+, to easily intercalate or deintercalate between the electrode surface and aqueous electrolyte, improving the electrochemical performance of the electrodes [44,45].

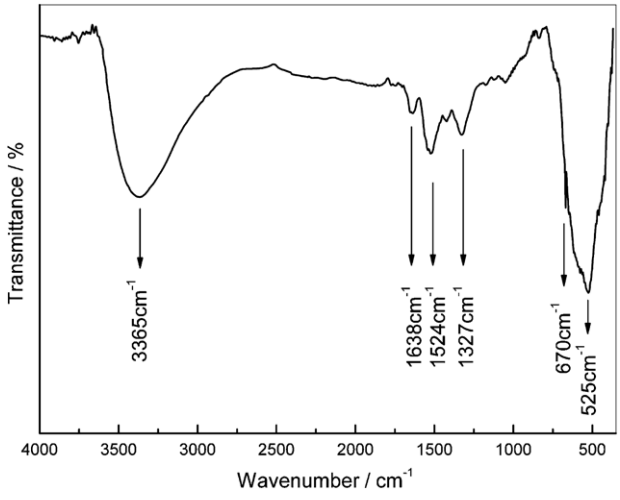

Fig. 6. FT-IR spectrum of the MnO_2 powders scraped from the substrate.

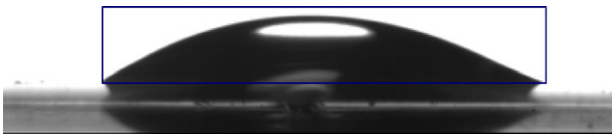

Fig. 7. Optical image of the water contact angle of the MnO_2 thin film deposited on the ITO/PET substrate.

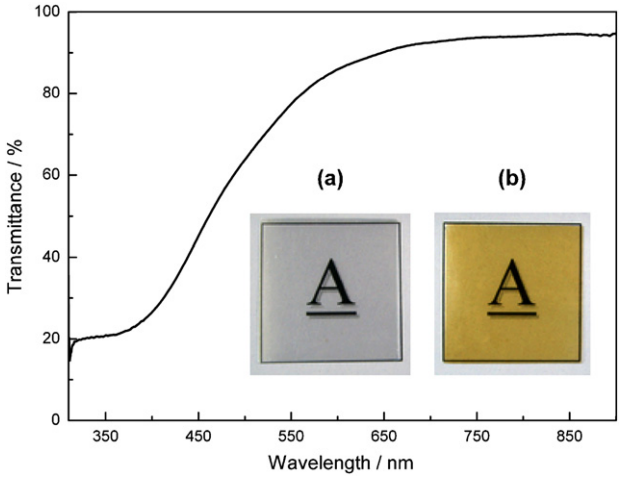

Fig. 8. Transmittance spectrum of the MnO_2 thin film deposited on the ITO/PET substrate. *Inset*: Photographs of (a) an ITO/PET substrate and (b) MnO_2 thin film electrode.

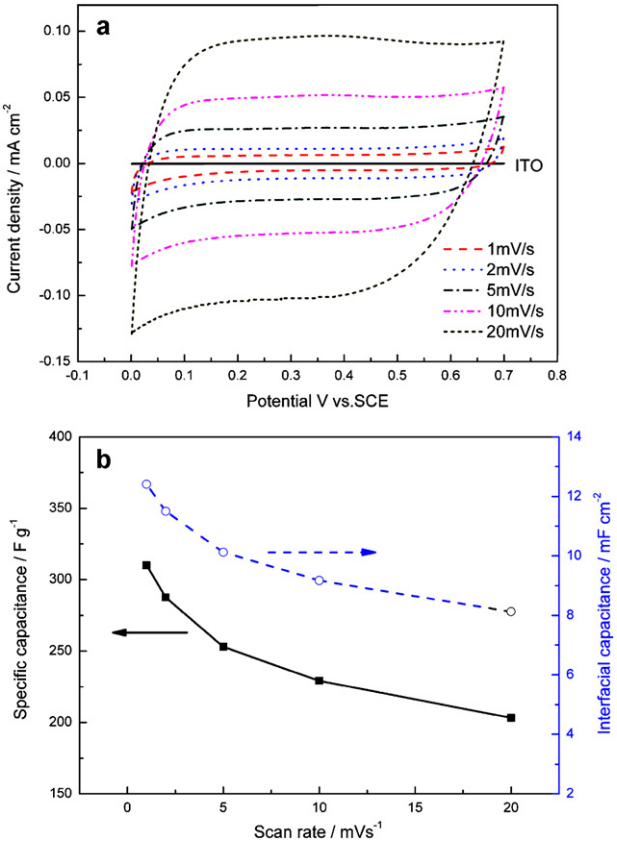

Fig. 9. (a) Cyclic voltammograms and (b) the specific and interfacial capacitances of MnO_2 thin film electrodes at different scanning rates.

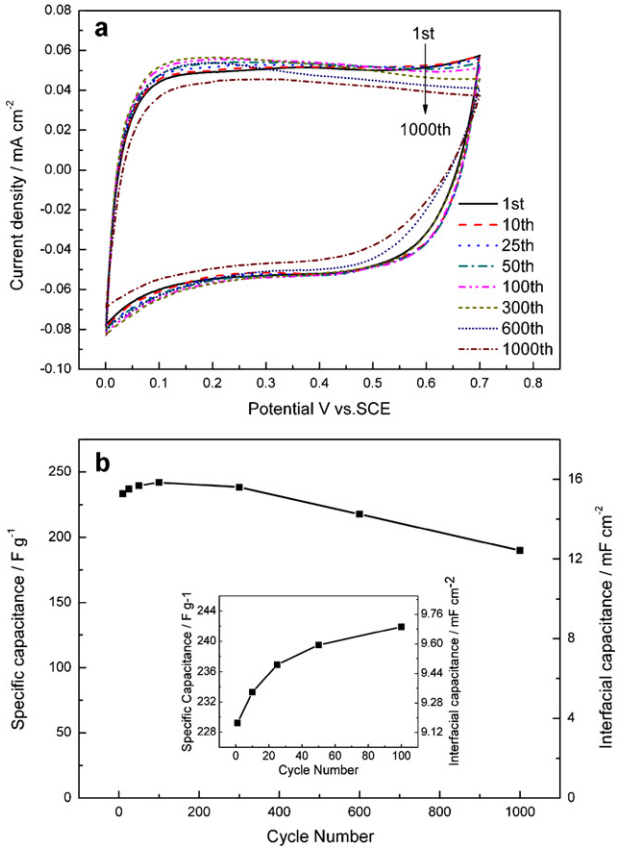

Fig. 10. (a) Cyclic voltammetry plots of the MnO_2 thin film electrodes at 10 mV s^{-1} and (b) specific and interfacial capacitances of the MnO_2 thin film electrodes.

Fig. 8 shows the transmittance spectrum of the MnO_2 thin film on the ITO/PET substrate. The transmittance of the thin film at 550 nm is up to 77.4%; this indicates the significant potential of the thin films' applications in transparent electrochemical capacitors. In comparison with previous methods, such as electrophoretic deposition, vacuum filtration and thin film transfer technology, our study has provided a much more simple and convenient method to fabricated thin films of even better optical performance, with less expensive active materials [13–15].

3.2.2. Electrochemical performances

The cyclic voltammogram and capacitance of the MnO_2 thin film electrodes were recorded at different scanning rates in Fig. 9. The rough symmetrical rectangle-like shape and rapid current response on potential reversal at each end of the electrode obtained as the sweep rates varied from 1 to 20 mV s^{-1} displayed ideal capacitive behavior (Fig. 9a). Compared with the MnO_2 thin film, the ITO substrate shows no capacitance. As the scan rate increased from 1 to

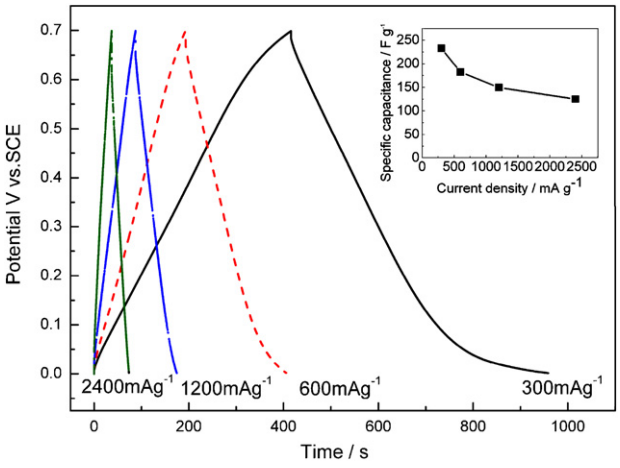

Fig. 11. Galvanostatic charge/discharge curves of the MnO_2 thin film electrodes at different current densities. *Inset*: Influence of the current density on the specific capacitance.

20 mV s^{-1}, the special capacitance and the interfacial capacitance decreased from 310 to 203.2 F g^{-1} and from 12.4 to 8.2 mF cm^{-2}, respectively (Fig. 9b).

Electrochemical stability is important for supercapacitors [2,7]. Fig. 10 displays the capacitance performances of the MnO_2 thin film electrode as a function of the cycle numbers at a scan rate of 10 mV s^{-1}. A specific capacitance retention ratio of 83% was obtained after 1000 cyclic voltammetry cycles, illustrating the long-term electrochemical stability of MnO_2 thin film electrodes. Interestingly, during the first 100 cycles, the specific capacitance slightly increased from 229.2 to 241.9 F g^{-1} (inset Fig. 10b), corresponding to the results of similar studies on γ-MnO_2 and Mg-doped Na birnessite-type MnO_2 [22,46].

The galvanostatic charge/discharge curves of the MnO_2 thin film electrodes are shown in Fig. 11 and their specific capacitances were calculated by Eq. (3). The symmetric shapes indicate the high reversibility and Coulombic efficiency of MnO_2 thin films [40]. Slight potential drops at the initial discharge stage were attributed to the electrical resistance of MnO_2 thin film and the diffusion limitation of the electrolyte. The specific capacitance value of the MnO_2 thin film, as indicated by the discharge curve, was 232.9 F g^{-1} at a current density of 300 mA g^{-1}. The specific capacitance of MnO_2 thin film electrodes was sustained at 125.2 F g^{-1} even when the charge/discharge current density was raised to eight times the original value (inset Fig. 11), because of the 3D porosity, layered structure, and large active surface area of the film.

3.2.3. Effects of bending angle and flexure count on electrochemical performances

The effects of bending angle and flexure count on the electrochemical capability of as-prepared MnO_2 thin film electrodes

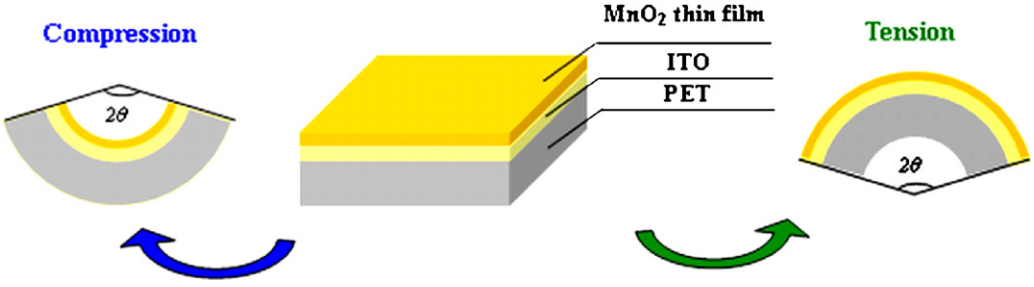

Fig. 12. Schematic of the bending test.

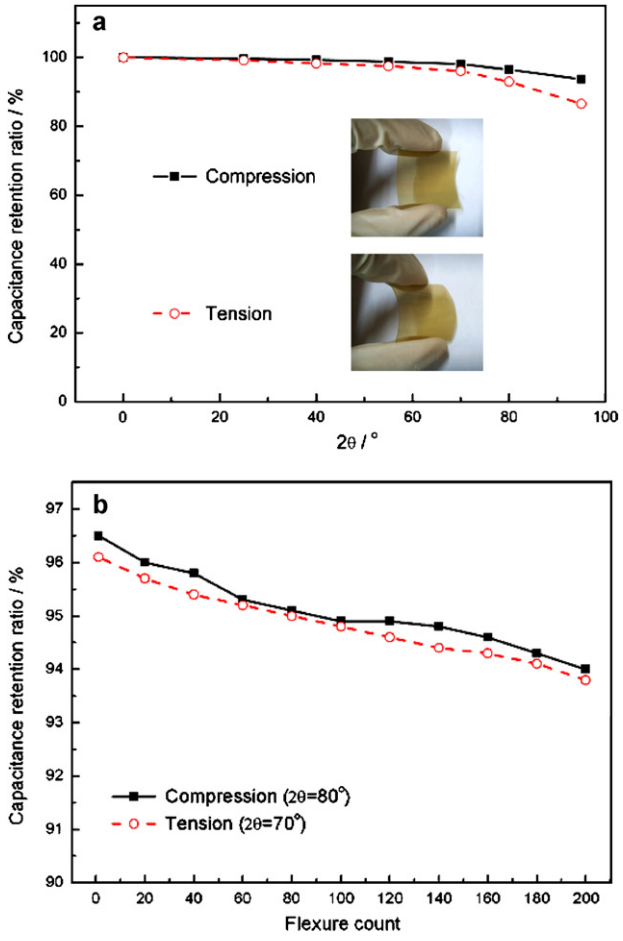

Fig. 13. Capacitance retention ratios of the MnO_2 thin film electrodes against: (a) the bending angle (2θ) and (b) the flexure count. Inset shows the optical images of the flexible MnO_2 thin films on ITO/PET substrates.

were systemically investigated because high performance under mechanically stressed conditions is of paramount importance in flexible devices [47]. Schematic illustrations of the compressive and tensile bending tests, and their results, are shown in Figs. 12 and 13, respectively. Under compressive strain, the bending angle should be no more than 80° to maintain a constant specific capacitance, and under tensile strain, the maximum bending angle should be 70° (Fig. 13a). If the bending angle for both compression and tension is further increased, the capacitance retention ratio value decreases to less than 96% of the original value. After bending for 200 cycles, only a slight decrease in specific capacitance was observed (2.5% at a bending angle of 80° under compressive strain, and 2.3% at a bending angle of 70° under tensile strain) (Fig. 13b), demonstrating the good mechanical flexibility and electrochemical stability of MnO_2 thin film electrodes under harsh bending conditions.

4. Conclusions

Transparent layered birnessite-type MnO_2 thin films are successfully fabricated on flexible and lightweight ITO/PET substrates through a facile, effective and inexpensive CBD method at room temperature. MnO_2 thin films of 40 $\mu g\,cm^{-2}$ prepared under optimum conditions of 0.1 M $KMnO_4$, 2:1 initial molar ratio of $NH_3{\cdot}H_2O$ and $KMnO_4$, 25 °C, and 12 h, featured 3D porous morphology, a water contact angle of 34°, and a specular transmittance of 77.4% at 550 nm. At a scan rate of 10 $mV\,s^{-1}$, the MnO_2 thin film electrodes exhibited a special capacitance of 229.2 $F\,g^{-1}$, an interfacial capacitance of 9.2 $mF\,cm^{-2}$, and a capacitance retention ratio of 83% after 1000 cyclic voltammetry cycles in 1 M Na_2SO_4. After bending for 200 cycles, only a small decrease in specific capacitance was observed, indicating the excellent mechanical flexibility and electrochemical stability of MnO_2 thin film electrodes.

Acknowledgements

This work was supported by the National Natural Science Foundation of China (No. 20876182), the Natural Science Foundation of Guangdong Province (No. 7003705), and the Science and Technology Project of Guangdong Province (No. 2010B010800022).

References

[1] V.S. Jamadade, V.J. Fulari, C.D. Lokhande, J. Alloys Compd. 509 (2011) 6257–6261.
[2] R.R. Bi, X.L. Wu, F.F. Cao, L.Y. Jiang, Y.G. Guo, L.J. Wan, J. Phys. Chem. C 114 (2010) 2448–2451.
[3] R.R. Salunkhe, K. Jang, H. Yu, S. Yu, T. Ganesh, S.H. Han, H. Ahn, J. Alloys Compd. 509 (2011) 6677–6682.
[4] D.P. Dubal, D.S. Dhawale, R.R. Salunkhe, V.S. Jamdade, C.D. Lokhande, J. Alloys Compd. 492 (2010) 26–30.
[5] T. Lu, L.K. Pan, H.B. Li, G. Zhu, T. Lv, X.J. Liu, Z. Sun, T. Chen, D.H.C. Chua, J. Alloys Compd. 509 (2011) 5488–5492.
[6] Y.J. Yang, E.H. Liu, L.M. Li, Z.Z. Huang, H.J. Shen, X.X. Xiang, J. Alloys Compd. 487 (2009) 564–567.
[7] J. Li, E.H. Liu, W. Li, X.Y. Meng, S.T. Tan, J. Alloys Compd. 478 (2009) 371–374.
[8] G.R. Li, Z.P. Feng, Y.N. Ou, D. Wu, R.W. Fu, Y.X. Tong, Langmuir 26 (2010) 2209–2213.
[9] Y.C. Chen, Y.K. Hsu, Y.G. Lin, Y.K. Lin, Y.Y. Horng, L.C. Chen, K.H. Chen, Electrochim. Acta 56 (2011) 7124–7130.
[10] Q. Wu, Y.X. Xu, Z.Y. Yao, A.R. Liu, G.Q. Shi, ACS Nano 4 (2010) 1963–1970.
[11] V. Presser, L.F. Zhang, J.J. Niu, J. McDonough, C. Perez, H. Fong, Y. Gogots, Adv. Energy Mater. 1 (2011) 423–430.
[12] P.C. Chen, G.Z. Shen, Y. Shi, H. Chen, C.W. Zhou, ACS Nano 4 (2010) 4403–4411.
[13] A.P. Yu, I. Roes, A. Davies, Z.W. Chen, Appl. Phys. Lett. 96 (2010) 253105.
[14] P.C. Chen, G.Z. Shen, S. Sukcharoenchoke, C.W. Zhou, Appl. Phys. Lett. 94 (2009) 043113.
[15] J. Ge, G.H. Cheng, L.W. Chen, Nanoscale 3 (2011) 3084–3088.
[16] S. Chen, J.W. Zhu, X.D. Wu, Q.F. Han, X. Wang, ACS Nano 4 (2010) 2822–2830.
[17] H. Xia, M.O. Lai, L. Lu, J. Power Sources 196 (2011) 2398–2402.
[18] D.P. Dubal, D.S. Dhawale, R.R. Salunkhe, C.D. Lokhande, J. Alloys Compd. 496 (2010) 370–375.
[19] Y. Lei, B. Daffos, P.L. Tabern, P. Simon, F. Favier, Electrochim. Acta 55 (2010) 7454–7459.
[20] Y. Chen, Y.Z. Hong, Y.P. Ma, J.B. Li, J. Alloys Compd. 490 (2010) 331–335.
[21] F. Li, J.F. Wu, Q.H. Qin, Z. Li, X.T. Huang, J. Alloys Compd. 492 (2010) 339–346.
[22] Y.M. Wang, H.F. Liu, M. Bao, B.J. Li, H.F. Su, Y.X. Wen, F. Wang, J. Alloys Compd. 509 (2011) 8306–8312.
[23] D.L. Fang, B.C. Wu, A.Q. Mao, Y. Yan, C.H. Zheng, J. Alloys Compd. 507 (2010) 526–530.
[24] W. Xiao, H. Xia, J.Y.H. Fuh, L. Lu, J. Electrochem. Soc. 156 (2009) A627–A633.
[25] S. Ching, D.J. Petrovay, M.L. Jorgensen, Inorg. Chem. 36 (1997) 883–890.
[26] X. Tang, H. Li, Z.H. Liu, Z. Yang, Z. Wang, J. Power Sources 196 (2011) 855–859.
[27] M.T. Martinez, A.S. Lima, N. Bocchi, M.F.S. Teixeira, Talanta 80 (2009) 519–525.
[28] Y. Dai, K. Wang, J. Xie, Appl. Phys. Lett. 90 (2007) 104102.
[29] G.D. Du, J.Q. Wang, Z.P. Guo, Z.X. Chen, H.K. Liu, Mater. Lett. 65 (2011) 1319–1322.
[30] L. Zhou, J. Zhang, J.H. He, Y.C. Hu, H. Tian, Mater. Res. Bull. 46 (2011) 1714–1722.
[31] M. Nakayama, T. Kanaya, J.W. Lee, B.N. Popov, J. Power Sources 179 (2008) 361–366.
[32] D. Wei, S.J. Wakeham, T.W. Ng, M.J. Thwaites, H. Brown, P. Beecher, Electrochem. Commun. 11 (2009) 2285–2287.
[33] Q. Liu, M.H. Nayfeh, S.T. Yau, J. Power Sources 195 (2010) 7480–7483.
[34] Y.J. Kang, B. Kim, H. Chung, W. Kim, Synth. Met. 160 (2010) 2510–2514.
[35] J.H. Zhu, J. Jiang, J.P. Liu, R.M. Ding, H. Ding, Y.M. Feng, G.M. Wei, X.T.J. Huang, Solid State Chem. 184 (2011) 578–583.
[36] M. Toupin, T. Brousse, D. Bélanger, Chem. Mater. 16 (2004) 3184–3190.
[37] E. Scavetta, A. Mignani, D. Prandstraller, D. Tonelli, Chem. Mater. 19 (2007) 4523–4529.
[38] P. Justin, G. Rao, Int. J. Hydrogen Energy 35 (2010) 9709–9715.
[39] K. Takahashi, Y. Wang, G.Z. Cao, J. Phys. Chem. B 109 (2005) 48–51.

[40] X.J. Yang, Y. Makita, Z.H. Liu, K. Sakane, K. Ooi, Chem. Mater. 16 (2004) 5581–5588.
[41] M.V. Ananth, S. Pethkar, K. Dakshinamurthi, J. Power Sources 75 (1998) 278–282.
[42] M. Ghaemi, F. Ataherian, A. Zolfaghari, S.M. Jafari, Electrochim. Acta 53 (2008) 4607–4614.
[43] Y.Q. Wang, A.B. Yuan, X.L. Wang, J. Solid State Electrochem. 12 (2008) 1101–1107.
[44] S.G. Kandalkar, C.D. Lokhande, R.S. Mane, S.H. Han, Appl. Surf. Sci. 253 (2007) 3952–3956.
[45] X. Li, X. Li, N. Dai, G. Wang, Z. Wang, J. Power Sources 195 (2010) 5417–5421.
[46] L. Athoüe, F. Moser, R. Dugas, O. Crosnier, D. Bélanger, T. Brousse, J. Phys. Chem. C 112 (2008) 7270–7277.
[47] K. Park, S.Y. Lee, S. Kim, J. Chang, S.J.L. Kang, K.J. Lee, Electrochem. Solid State Lett. 13 (2010) G57–G59.